J. Fluid Mech. (2001), *vol.* 448, *pp.* 175–195.
DOI: 10.1017/S0022112001005985 Printed in the United Kingdom

Vortex-induced vibrations of a cylinder with tripping wires

By F. S. HOVER, H. TVEDT AND M. S. TRIANTAFYLLOU

Department of Ocean Engineering, Massachusetts Institute of Technology, Cambridge, MA 02139, USA

(Received 20 December 1999 and in revised form 1 June 2001)

Thin wires are attached on the outer surface and parallel to the axis of a smooth circular cylinder in a steady cross-stream, modelling the effect of protrusions and attachments. The impact of the wires on wake properties, and vortex-induced loads and vibration are studied at Reynolds numbers up to 4.6×10^4, with 3.0×10^4 as a focus point. For a stationary cylinder, wires cause significant reductions in drag and lift coefficients, as well as an increase in the Strouhal number to a value around 0.25–0.27. For a cylinder forced to oscillate harmonically, the main observed wire effects are: (*a*) an earlier onset of frequency lock-in, when compared with the smooth cylinder case; (*b*) at moderate amplitude/cylinder diameter (A/D) ratios (0.2 and 0.5), changes in the phase of wake velocity and of lift with respect to motion are translated to higher forcing frequencies, and (*c*) at $A/D = 1.0$, no excitation region exists; the lift force is always dissipative.

The flow-induced response of a flexibly mounted cylinder with attached wires is significantly altered as well, even far away from lock-in. Parameterizing the response using nominal reduced velocity $V_{rn} = U/f_nD$, we found that frequency lock-in occurs and lift phase angles change through 180° at $V_{rn} \approx 4.9$; anemometry in the wake confirms that a mode transition accompanies this premature lock-in. A plateau of constant response is established in the range $V_{rn} = 5.1$–6.0, reducing the peak amplitude moderately, and then vibrations are drastically reduced or eliminated above $V_{rn} = 6.0$. The vortex-induced vibration response of the cylinder with wires is extremely sensitive to angular bias near the critical value of $V_{rn} = 6.0$, and moderately so in the regime of suppressed vibration.

1. Introduction

Protrusions, structural imperfections, and attachments on the surfaces of bluff cylinders are known to have a considerable effect on the vortex formation process, and hence on the loads and resulting oscillations of flexibly mounted cylinders. In most applications involving bluff cylinders, such as marine cables and risers, towed tethers, chimney stacks, and bundles of conducting pipes, the surfaces contain imperfections. Furthermore, structural supports, auxiliary pipes in marine risers, attachments, connectors, and surface ridges or grooves created by helically wound cables or ropes, invariably introduce surface imperfections that disturb the nominally smooth flow. While the complexities of the imperfections play a role in the changes of the flow structure, the basic impact of the imperfection is in tripping the boundary layer, causing potentially substantial changes in the separation point, especially at higher Reynolds numbers.

Fage & Warsap (1929) first studied the effect of small protrusions on non-oscillating cylinders, and showed that certain configurations of thin wires, stretched parallel to the cylinder axis, or rough paper, reduce the drag coefficient and alter the pressure distribution. These effects are pronounced even when the wire diameters and roughness scales are smaller than the laminar boundary layer thickness, and they are enhanced at higher Reynolds numbers. Fage & Warsap further noted the qualitative and sometimes quantitative similarities between the changes caused by the protrusions, and changes brought about by natural flow transition at a critical Reynolds number near 2.5×10^5. Others have studied stationary, or slightly moving, cylinders in supercritical flow, including Fung (1960), Roshko (1961), Jones, Cincotta & Walker (1968), Bearman (1969), Schewe (1983), and Shih *et al.* (1993). The principal characteristic of the flow as the Reynolds number reaches the critical value is a dramatic reduction in drag coefficient from 1.2 to about 0.3, and then a recovery to a value of about 0.5–0.7 in the transcritical regime above $Re \simeq 3.5 \times 10^6$. These variations are correlated with a wake width that varies with Reynolds number.

The effect of wires on the flow over a subcritical cylinder has been studied more recently by James & Truong (1972) and Igarashi (1986), who considered a number of different wires and placement angles with respect to the stagnation point. Igarashi further classified the results into three distinct patterns, and flow visualization showed that the various drag and pressure trends relate directly to distinct flow separation conditions. The flow may either (*a*) relaminarize beyond the wire, (*b*) immediately form a turbulent boundary layer, or (*c*) separate at the wire. Results in the second case resemble the naturally occurring critical flow at a much higher Reynolds number, whereas the flow in the first case resembles that of a smooth cylinder, and in the third case an abnormally early separation occurs. Igarashi found that turbulent boundary layers are created near the same angles employed by Fage & Warsap (1929), i.e. near $\pm 65^\circ$. The strong local flow disturbance and early transition to turbulence in the boundary layer caused by the wires thus provides an explanation for the phenomena observed, and for the similarity with the characteristics of high Reynolds number flows. The use of thin wires on an otherwise smooth cylinder has also received attention in the area of tube bundles: recent work by Romberg & Popp (1998), for example, parameterizes the stability properties of a single flexible tube embedded in a heat exchanger bundle, with and without tripping wires.

It is tempting to model the flow around cylinders at critical and supercritical Reynolds numbers through the appropriate use of wires at lower Reynolds number values. Building on the results of Fage & Warsap (1929), however, Pearcey, Cash & Salter (1982) showed that while some of the drag and mean pressure characteristics of subcritical cylinders with wires match those of true supercritical flow, there are serious difficulties encountered at the lower Reynolds numbers, where the wires must be quite large to achieve the desired effect. In addition, no systematic data exist for cylinders oscillating at high amplitude in the supercritical regime, and until they become available, the hypothesis that the effect of trip wires can accurately model the natural transition cannot be tested.

Because trip wires alter subcritical flows nonetheless, they are also suggested as a possible means for controlling the flow around cylinders. One idea proposes using the effect of wires or protrusions for the reduction of drag and potentially of vortex-induced vibrations (VIV), at a high but subcritical Reynolds number. The use of wires on cylinders undergoing VIV, however, has not been studied extensively, even at low Reynolds numbers; an exception is the work of Price (1956), who found that for free vibrations at $Re = 4.6 \times 10^3$, trip wires had very little influence on the large-scale VIV

motions. This Reynolds number, though, is well below the threshold values found in the earlier study as necessary for altering drag substantially. Zdravkovich (1981) rejects wires as a strategy for attenuating VIV based on Price's tests, but also because of the possible inherent sensitivity to flow direction relative to the wires.

In this paper, we identify several significant effects of the wires with respect to VIV, both on the measured forces and on vortex-induced motions of a circular cylinder. The three sets of data presented are summarized as follows: (*a*) drag tests with no cylinder vibration: $Re = 1.5$–4.6×10^4, (*b*) forced vibrations at $Re = 3.0 \times 10^4$, and (*c*) free vibrations at $Re = 3.0 \times 10^4$. The stationary cylinder tests were performed mainly as a check of the equipment and as a context for the other experiments.

All of the tests have been performed both with and without wires, under otherwise identical conditions, so that the effects of the wires are made clear. A review of the known properties of smooth cylinders in VIV is thus appropriate. Forced-vibration results for smooth cylinders in subcritical flow can be characterized by a lock-in region of frequency and amplitude, within which the wake frequency is captured by the frequency of the imposed oscillation (e.g. Bishop & Hassan 1964; Karniadakis & Triantafyllou 1989). Additionally, there are at least two stable wake patterns which may form, depending on the amplitude and frequency of oscillation: one with two single vortices shed per cycle, denoted as a '2S' mode, and another with two pairs of vortices per cycle, denoted as a '2P' mode by Williamson & Roshko (1988). The appearance of these two modes in free vibrations has been demonstrated by Brika & Laneville (1993), who studied air flow past a flexible circular beam and also found two major branches of response which accounted for the hysteresis noted by previous researchers. The upper branch is primarily a '2S' mode whose loci fall in the '2P' region defined by Williamson & Roshko; the lower branch is a '2P' mode that traverses this same region. The transitions between these branches are marked by sharp changes in amplitude, changes in the phasing between lift force and displacement from near zero to near 180°, and the appearance of a free-vibration lock-in phenomenon, i.e. the linking of the observed frequency of vortex formation to the structural mode instead of to the natural Strouhal frequency (Feng 1968).

A case of low structural damping (damping ratio $\zeta \simeq 1 \times 10^{-4}$) is described by Khalak & Williamson (1997), for a rigid cylinder in water. Observations are made of the same hysteretic branches noted above, and additionally of a rapid switching of modes at the onset of lock-in, indicated by a varying phase angle between transverse force and displacement. Additionally, at even lower mass and damping, a third branch appears (Govardhan & Williamson 2000). Hover, Techet & Triantafyllou (1998) show, by measuring the forces at both ends of the test cylinder, that in the region where transition is expected, the lift forces become uncorrelated. This loss of correlation, in a region where substantial vibrations occur, is attributed to the formation of mixed (*hybrid*) modes, consisting partially of a lower branch mode, and transitioning through a vortex split to an upper branch mode at some point along the span of the cylinder. Flow visualization in Techet, Hover & Triantafyllou (1998) shows the detailed structure of a '2S/2P' hybrid mode.

2. Experimental setup

2.1. *Physical description*

Tests were conducted at the MIT Testing Tank facility, a 30 m × 2.5 m × 1.2 m still-water towing tank; the physical arrangement has been described in Hover *et al.* (1998).

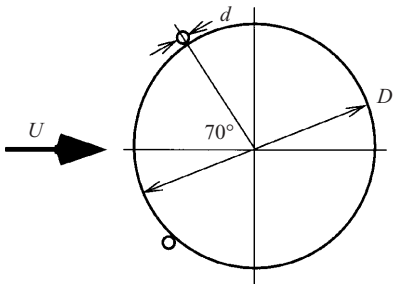

FIGURE 1. Wire locations on the rigid circular cylinder, at $\pm 70^\circ$ from the stagnation point.

We used a rigid aluminium cylinder with diameter $D = 7.62\,\text{cm}$ and span $L = 200\,\text{cm}$, moving at constant speed horizontally while oscillating transversely to the flow (in the vertical direction). The blockage ratio in the tank is approximately 4%. At each end of the cylinder there is a 0.2 cm gap to a 31 cm diameter end-plate, and it is supported by a pair of three-axis Kistler piezo-electric load cells, which are in turn attached to a heaving structure that also supports the end-plates. This assembly is positioned using an ALM lead screw with 30 cm travel, driven by a Parker-Hannafin brushless servomotor. The motor is controlled from a personal computer equipped with an MEI motion control card and a C++ programming environment. A TSI conical constant-temperature anemometer (CTA) was employed for many of the runs, at a fixed location two diameters downstream, and one diameter lateral to the cylinder's mean centreline position. The system described so far sits on a mobile carriage, whose velocity through the water is controlled independently by a separate computer.

A 7-channel data bus connects the carriage with a third (stationary) personal computer, which logs the following analog data: absolute vertical position of the cylinder assembly (Shaevitz LVDT), motor shaft position converted to volts, drag and lift at each end of the cylinder (4 channels, analog filtered at 33 Hz), and the anemometer signal. We use DasyLab data acquisition software to collect data in IEEE 32-bit format, and then post-process in a Matlab environment.

Steel wires, parallel to the cylinder axis, were attached to miniature turnbuckles, and stretched over small notches cut into the cylinder ends. We applied a tensile load of approximately 50 N, which was sufficient to keep the wire tight against the cylinder wall; no glue or other method was used to hold the wire against the cylinder. We employed wires of diameter $d = 0.23\,\text{mm}$, located at $\beta = \pm 70^\circ$ with respect to the stagnation point; see figure 1. This leads to a wire to cylinder diameter ratio of $d/D = 0.0030$, and the range of values $d/\delta = 0.39$–0.77, where δ is the boundary layer thickness at the location of the wire, after Pohlhausen (Schlichting 1979). Note that this wire location does not necessarily correlate with the greatest drag reduction, as Igarashi (1986) reports mean C_d values as low as 0.39 for large wires at $\beta = \pm 50^\circ$. We chose a larger separation angle so that the properties induced by the wires might be more robust against oscillation, which rotates the incident velocity vector, and also against misalignment. Table 1 gives wire sizing and placement parameters for several comparable studies.

The non-oscillating tests involved variations in towing speed only. The forced vibration tests were conducted at constant speed, while varying both the amplitude of motion and the frequency. Free vibration tests were also performed at constant speed, while nominal reduced velocity, defined below, was varied.

	d/D	d/δ	β (deg.)
Fage & Warsap (1929)	0.0002–0.0033	0.0270–1.17	± 65
Pearcey *et al.* (1982)	0.0039–0.039	0.48–32.6	± 40, ± 50
Igarashi (1986)	0.0080–0.0294	0.65–8.22	± 50, ± 60
Present tests	0.0030	0.39–0.77	± 70

TABLE 1. Parameters of comparable studies.

2.2. *Control system and damping*

In the case of sinusoidally oscillating tests, the servomotor executes commands of the form $y(t) = A\cos\omega t$, and the seven data channels can be recorded directly. For free vibrations, we employed a robotic force-feedback loop that is a hybrid simulation–experiment, as described in Hover *et al.* (1998) and Hover & Triantafyllou (1999). In this case, the lift force measurements are fed into the computer on the carriage, a real-time simulation of a compliant structure is executed, and the output is used to drive the servomotor trajectory. The force–control system update interval is 2 ms, while the servomotor loop runs at about 0.3 ms.

In the present experiments the modelled system consists of a mass–dashpot–spring system. The simulation mass M, damping B, and stiffness K can all be specified by the user, thus allowing the variation of nominal reduced velocity $V_{rn} = 2\pi U/\omega_n D$ at constant towing speed and Reynolds number; $\omega_n = \sqrt{K/M}$ is the undamped natural frequency of the virtual structure. Intrinsic in the feedback loop is a correction for that component of measured force that is due to the inertia in the material test cylinder; this mass is effectively replaced with M by adding to the measurement the term $m_{cylinder}\ddot{y}$. The data in the current work were obtained with the non-dimensional mass ratio $m^* = 4M/\rho\pi D^2 L = 3.0$, and a nominal damping ratio of zero.

The compensator takes specific account of phase losses due to the servomotor, analog filtering, and also of a lightly damped resonant mode in the carriage structure at about 138 rad s^{-1}. However, this mode, along with other effects such as backlash in the lead screw assembly, cannot be eliminated with notch filters alone, and some additional limitations on closed-loop bandwidth are required to keep the cylinder motion smooth. These constraints induce a small, unavoidable amount of damping. Under sinusoidal force excitation, the target system for the present free-vibration tests has the specific magnitude and phase characteristics shown in figure 2, wherein we also indicate the ideal properties of a pure mass–spring system (no damping), and those of a second-order system with a damping ratio of $\zeta = 0.032$. The target natural frequency and damping ratio (with $V_{rn} = 5.5$) are 7.50 rad s^{-1} and 0.026, respectively; this damping is the lowest that can be achieved in the design. Experimental tests in air confirmed values of 7.51 ± 0.01 rad s^{-1}, and 0.032 ± 0.005, demonstrating that the performance of the implemented closed-loop system is quite good. Nonetheless, it is apparent that our target system itself does not faithfully replicate the phase characteristics of the damped second-order case, and that some additional description of the system is required.

The second-order linear transfer function has the form $y(s)/F(s) = 1/(Ms^2+Bs+K)$, where y denotes displacement, F the applied force, and $\{M, B, K\}$ are the mass, dashpot, and spring; s is the Laplace variable. The phase angle of the force with respect to the displacement is therefore $\phi = \arctan(B\omega/(M\omega^2 - K))$, and for small ζ a good approximation is $\phi \simeq 2\zeta(1+\sigma)/\sigma(2+\sigma)$, where $\sigma = (\omega - \omega_n)/\omega_n$, the

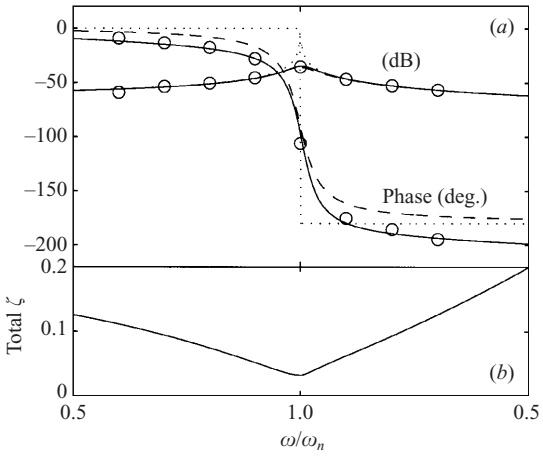

FIGURE 2. (*a*) Magnitude and phase plots of an ideal undamped mass–spring system (···), the target system in the feedback loop (—), the results of pluck experiments in air (○), and a mass–spring–dashpot system with 3.2% damping (——). The phase discrepancy between the target and the damped second-order system leads to a frequency-dependent net damping ratio whose lowest value is targeted at lock-in (*b*).

non-dimensional perturbation from the natural frequency. Hence, the phase angle is linear in ζ and we may describe an effective, or total, damping ratio that is a function of frequency. For the conditions of this discussion, the total damping ratio is shown in figure 2(*b*). Prior to lock-in, where the frequency of vibration is substantially below the structure's natural frequency, ζ may be as high as 0.12, at a value of $\omega/\omega_n \simeq 0.5$, where vibrations first start to occur. Lock-in occurs near ω_n, and at this point damping is at its minimum value, and close to the value we have observed in air. At higher frequencies of motion, again the damping ratio increases, although probably not above 0.10, based on frequency data presented in what follows.

To summarize, the closed-loop feedback system imposes bandwidth constraints which lead to a phase loss that can be modelled as a damping ratio that varies with frequency. Away from the resonant point, the damping observed in VIV experiments is as high as 0.12, which leads to significant phase angles in the results. At the resonant frequency, a damping ratio of 0.032 has been observed, and thus $m^*\zeta = 0.096$. In general, the amplitude of motion we observe at lock-in, $A/D \approx 0.94$, is on the low side of the data compiled by Khalak & Williamson (1999).

2.3. *Data processing*

We measured the motion and the lift and drag forces at both ends of the cylinder, and the wake in-line velocity. All calibrated time series were detrended (zeroth- and first-order components removed from a polynomial fit), and then low-pass filtered with zero phase, using a fourth-order Butterworth design of bandwidth 30 rad s^{-1}. The data acquisition sampling interval was 10 ms. Data were processed after each run, and the following quantities were calculated:

for free vibrations, the average 1/10th-highest amplitude/diameter ratio $A/D_{1/10}$;

total lift coefficient $C_l = 2F/\rho DLU^2$, constructed from the magnitude F of the total lift force;

phase angle ϕ_F between the oscillating lift force and the imposed motion, and corresponding phase angle ϕ_A between the anemometer trace and the motion;

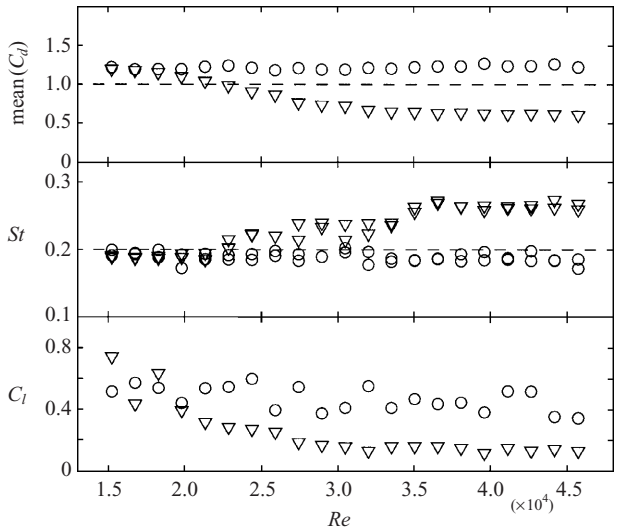

FIGURE 3. Mean drag coefficient, Strouhal number, and lift coefficient magnitude properties of a non-oscillating cylinder, with (▽) and without (○) trip wires. The plot shows Strouhal numbers based on both the lift force and the anemometer signals.

peak spectral frequencies of the motion (ω), the lift force on the cylinder (ω_F), and the anemometer (ω_A);

correlation coefficient F_c of the two end lift force signals;

mean drag coefficient, mean(C_d);

standard deviation of the drag coefficient, std(C_d);

lift coefficient in phase with acceleration, $C_{la} = -C_l \cos\phi_F$;

added mass coefficient, $C_m = -2U^2 C_{la}/\pi\omega^2 D^2(A/D)$;

lift coefficient in phase with velocity, $C_{lv} = C_l \sin\phi_F$.

Lift forces are corrected for the inertial effect of the solid (sealed) cylinder, through the equation

$$F_{lift} = F_{measured} + m_{cylinder}\ddot{y}(t).$$

For the parametric data presented, we show the average of force coefficients computed for each end of the cylinder. Lift and drag coefficients are not corrected for blockage effects. ϕ_F is shown as a sum of the end values, weighted with the lift forces. In the figures where we present measured time traces, force data are given for both ends of the cylinder.

Many of the signals are broadband by nature, most notably that of the anemometer. This led to some scatter in selection of the peak frequencies. Additionally, phase angles were computed using an inner product, over many data bins containing one motion period. The statistics of this iterative approach are shown in the phase figures that follow, as error bands of plus and minus one standard deviation from the mean values. We applied an arbitrary constant offset to ϕ_A, in order to align it with ϕ_F in the figures.

3. Results

3.1. *Stationary cylinder*

The addition of wires to a non-oscillating smooth cylinder causes several immediate changes in the flow characteristics, especially in the upper speed range considered.

As seen in figure 3, the mean drag coefficient of a cylinder with wires undergoes a gradual reduction with increasing Reynolds number, from the subcritical smooth-cylinder value of around 1.2, to a minimum value of 0.6 occurring above $Re = 3.5\times10^4$. As noted in the Introduction, this curve does not indicate the lowest drag values that can be obtained with wires; nonetheless, this drag transition agrees well with the references of table 1. Drag reduction here results from the generation of turbulence by the wires in the boundary layer, which causes separation at a higher angle along the cylinder circumference, reducing the wake width (Igarashi 1986). This effect is qualitatively similar to the natural transition, for which turbulence develops at increasingly advanced locations (that is, toward the stagnation point) on the cylinder as the velocity increases (Roshko 1961).

The lift coefficient amplitudes obtained with wires reach a minimum of about 0.15 (commensurate with oscillating drag, not shown), while, in contrast, the smooth cylinder has scattered values around 0.5. These lift properties are in good agreement with Jones *et al.* (1968), for a supercritical smooth cylinder at $Re = 3 \times 10^6$, with Ribeiro (1991), for rough cylinders, and with Gopalkrishnan (1992) for a subcritical smooth cylinder. The Strouhal number associated with the wires takes values in the range of 0.25–0.27, for the conditions of reduced drag, i.e. $Re \geqslant 3.5 \times 10^4$. As with the drag coefficient, variation from the smooth-cylinder value of 0.19 is generally continuous with Reynolds number. Both Igarashi (1986) and Pearcey *et al.* (1982) report values closer to 0.30 for a cylinder with wires.

The forced and free vibrations described next were studied at $Re = 3 \times 10^6$, in a 'critical' regime for the cylinder with wires, where the flow is still undergoing a fundamental transformation. Therefore, one important limitation of the current experiments is that the VIV response is likely to vary strongly with *Re*. On the subcritical side, we should expect that with reduced *Re*, say for $Re < 2 \times 10^4$, the response is close to that of the smooth cylinder. At higher *Re*, say $Re > 4 \times 10^4$, the sensitivity to *Re* could be reduced, but still the lack of data on supercritical VIV prohibits any rational prediction of the behaviour. As we show below, the response at $Re = 3 \times 10^4$ with wires is dissimilar from that of the subcritical smooth cylinder; the great majority of controlled studies on VIV are for the subcritical regime.

3.2. *Forced vibrations: drag and lift*

We conducted forced vibration tests at $Re = 3.0 \times 10^4$ for a range of reduced frequencies, and for four A/D ratios (0.1, 0.2, 0.5, 1.0). This value of *Re* is toward the upper end of, and still within, the drag transition zone, and hence the results below are dependent on Reynolds number.

The force, frequency, and phase results are plotted in figures 4–6. At the lowest amplitude, the drag coefficient associated with wires has a minimum value near 0.80, which grows with reduced frequency $f_r = \omega D/2\pi U$ but remains uniformly lower than without wires, where the value is around 1.2. The fact that drag is reduced for small-amplitude vibrations when wires are used can be attributed again to the tripping of the boundary layer and hence reduction of the wake width, as found in non-oscillating cylinders. For this small amplitude, the variation of the incident flow direction is only about $\pm7^\circ$. At $A/D = 0.2$ and upwards, mean drag on the smooth cylinder increases sharply near the lock-in frequency value of about 0.17 (Bishop & Hassan 1964; Sarpkaya 1977). The cylinder with wires shows a similar trend, but with a peak drag coefficient near $f_r = 0.20$, for $A/D = 0.2$ and 0.5. As the amplitude increases further, peak drag values become comparable to the smooth cylinder values. The wires thus provide mean drag reduction relative to a smooth cylinder for the

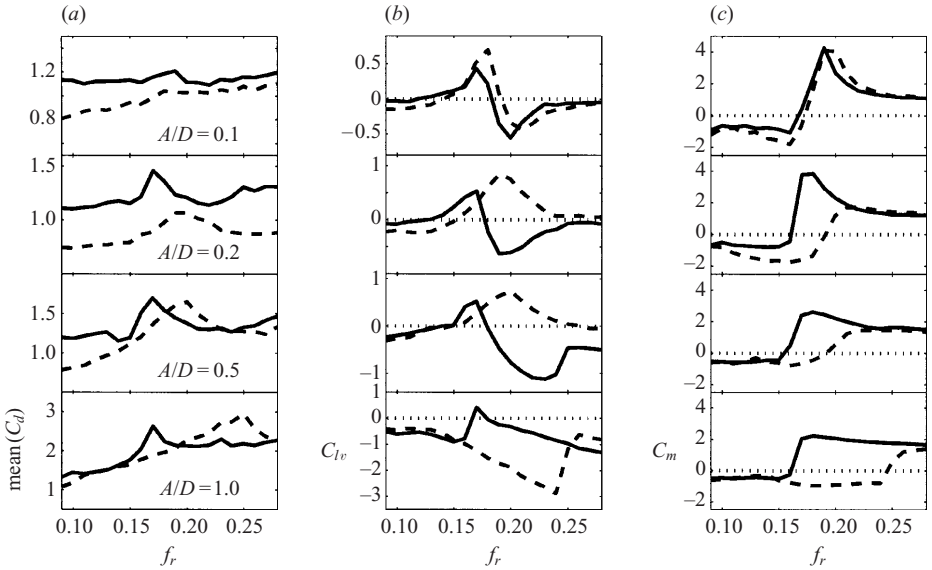

FIGURE 4. (*a*) Mean drag coefficient, (*b*) lift in phase with velocity, and (*c*) added mass coefficient, during forced oscillation tests. Smooth cylinder (—); wires (– –).

smaller amplitudes of motion, especially if the frequency of oscillation is less than the peak value for the cylinder with wires. Above this frequency, the drag values of the smooth cylinder and the cylinder with wires are expected to coincide as the effects of the wires are lost. This coincidence is likely to be reinforced further as the amplitude increases, since the incidence angle variation grows with both f_r and A/D.

With respect to lift forces, at $A/D = 0.1$ the wires have little effect, and the two curves for C_{lv} and C_m are very close. The smooth cylinder C_{lv} data here are similar to those reported elsewhere: there exists an excitation region (positive C_{lv}) in the range $f_r = 0.12$–0.17, with maximum C_{lv} values of around 0.5 at $f_r \simeq 0.16$. As the amplitude of motion increases, especially beyond $A/D = 0.5$, the excitation region shrinks to a small range near $f_r = 0.17$; this point of vanishing excitation region is regarded as a good prediction of the peak motions during VIV. It should be noted that in general, however, the VIV response depends on both the magnitude and slope of the lift curve with f_r, as well as the phase, so that we are discussing here a simplified case.

The addition of wires at larger A/D first moves the excitation region to higher frequencies, say $f_r = 0.16$–0.24 for $A/D = 0.2$, and also increases the C_{lv} magnitude to about 0.8, for $A/D \leqslant 0.5$. Based on these results for low A/D alone, it could be expected that the wires are likely to exacerbate VIV. At the highest amplitude we tested, $A/D = 1.0$, however, a dramatic change in C_{lv} occurs. There is *no* excitation region visible, as the maximum value attained is -0.22, at very low frequencies. Indeed, the entire shape of the curve, which for lower A/D looks like an extension of the excitation range, is altered. A fundamental modification of the flow, probably related to the angular deflection of the incident flow, which for $A/D = 1.0$ and $f_r = 0.20$ is approximately $\pm 51°$, makes free vibrations at this large amplitude unlikely. A more continuous change is evident in C_m. Here, the transition from negative to positive values moves to higher f_r as the amplitude of motion increases. For the smooth cylinder, this point seems to be stationary at $f_r \approx 0.16$. At very high frequencies, added mass dominates for both cylinders, forcing C_m to around 1.0–1.5.

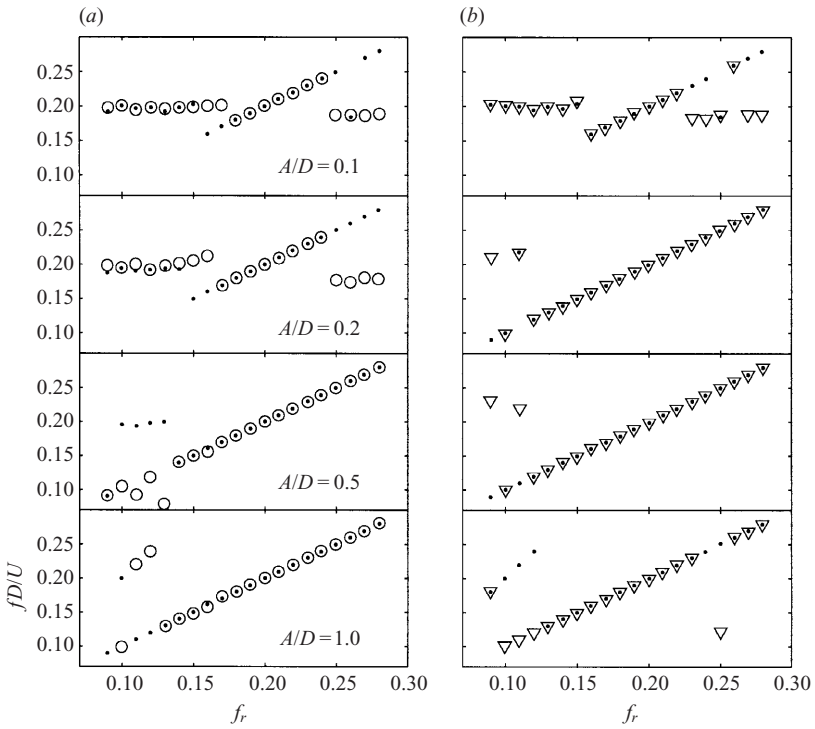

FIGURE 5. Non-dimensional peak frequency of the anemometer signal (○, △) and the lift force (·) during forced vibrations; (*a*) smooth, (*b*) wires.

Phase changes in lift force provide a rough indicator of mode changes in the wake, but since these measurements by nature include an uncertain added mass component, they cannot be used directly to ascertain the wake type. The anemometer signal is more appropriate in this regard. For the lower amplitudes, comparison of the lift and wake phases is good for both cylinders, and a mode change is clearly concomitant with the phase changes observed; see figure 6. With regard to the map of Williamson & Roshko (1988) these phase changes are typical of the division between '2S' (lower frequency) and '2P' (higher frequency) modes. The phase changes are more gradual for the cylinders with wires, and we note that the error statistics are best precisely in the transition zone.

At $A/D = 1.0$, ϕ_F and ϕ_A are in clear disagreement for the smooth cylinder, indicative of the increased role of added mass in the signal during these large motions. Phase angles with the wires attached are also not in good agreement at $A/D = 1.0$, and especially for $f_r > 0.15$, where a gap widens from about 30° to 130° at $f_r = 0.24$. At $f_r = 0.25$, both the lift and wake phase angles change dramatically, however, directly to the smooth cylinder values. C_{la} and C_m realign at this point also, suggesting that the effects of the wires are suddenly lost entirely.

3.3. *Forced vibrations: lock-in*

In the context of forced vibrations, lock-in has typically been defined as the locking of the primary wake frequency to the frequency of motion. Concurrent force measurements allow for a related lock-in measure, which involves the primary frequency of the lift force signal. Below we discuss both properties; the first we call *wake lock-in*, and the second *lift lock-in*. Within either definition, we further note that conventional

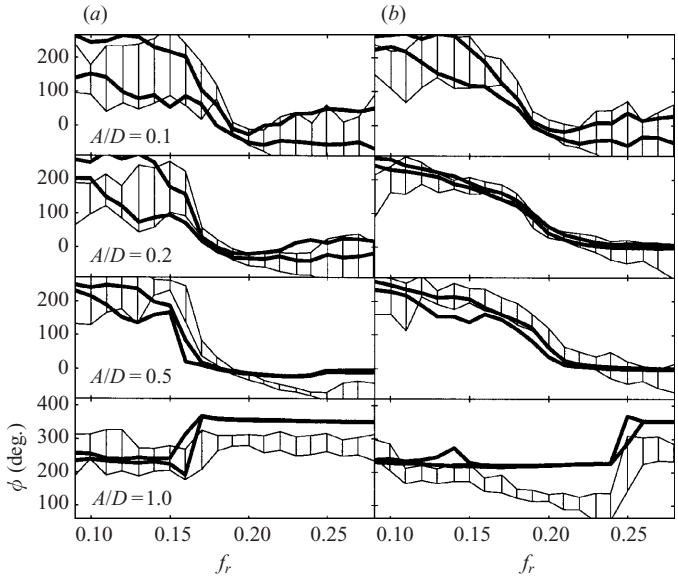

FIGURE 6. Phase angles during forced vibrations. Heavy solid lines show the mean value of ϕ_F plus or minus one standard deviation from windowed calculations. The hatched region denotes the identical spread for ϕ_A. (*a*) Smooth, (*b*) wires.

lock-in is said to exist when there are *no* traces of the natural shedding frequency ω_S in the wake or lift spectra. Conversely, if there is a significant component of ω_S in the spectra, we say that a non-lock-in condition exists.

For the present analysis, we made lock-in calculations using the *peak* frequencies of the wake velocity and lift forces. This was necessitated by some broadband signals, for which the role of ω_S cannot always be clearly discerned. We plot in figure 5 these (non-dimensionalized) frequencies. There are points for which the wake and lift values are in disagreement, and this is generally due to competing peaks; furthermore, the lift force contains added mass, and so has a propensity to follow the oscillation more closely at higher forcing frequencies.

The smooth-cylinder data show that wake and lift lock-in to the oscillation frequency occur fully at $f_r \simeq 0.18$, 0.17 and 0.14, for the three lowest amplitudes $A/D = 0.1$, 0.2 and 0.5, respectively. At $A/D = 1.0$, lock-in is suggested throughout the range of f_r tested, with the lowest frequency tests exciting a second harmonic of the motion in the wake, and close to the natural shedding frequency. Smooth-cylinder tests by Gopalkrishnan (1992) confirm a lower boundary for lock-in at $f_r = 0.16$, for amplitudes comparable to the ones considered here, and $Re = 1 \times 10^4$. On the other hand, Stansby (1976) conducted tests in air near the same Reynolds number, and found a significantly wider lock-in region, whose lower boundary is close to what we observe with the wires attached (below). Öngoren & Rockwell (1988) show similarly, for cylinders in air and for somewhat lower values of *Re*, an even wider range, with lock-in occurring down to $f_r/S = 0.6$, for $A/D = 0.13$.

In the present experiments, coincident wake and lift lock-in for the smooth cylinder then persists to $f_r = 0.19$ for $A/D = \{0.1, 0.2\}$, and then all the way to $f_r = 0.28$ for $A/D = \{0.5, 1.0\}$. Some variation again exists with the three references above, because of differing conditions.

With wires attached, the lowest amplitude motion results in wake and lift lock-in

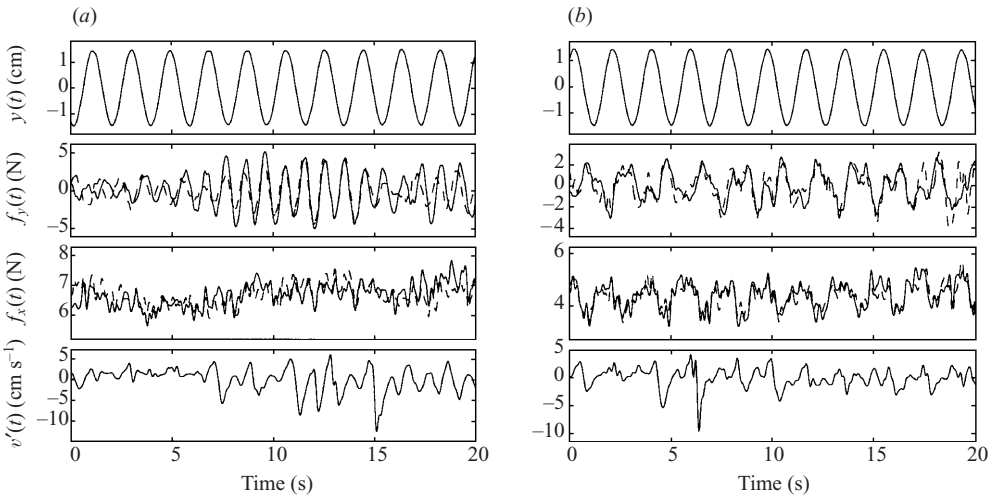

FIGURE 7. Time-domain traces of motion and forces during forced vibrations with (*a*) the smooth and (*b*) wired cylinders; $A/D = 0.20$, $f_r = 0.10$.

near $f_r = 0.16$, but during larger motions, lift and wake lock-in are evident at much lower frequencies than for the smooth cylinder. Specifically, the lock-in exists at and above $f_r = 0.12$ for $A/D = 0.2$ and 0.5; this represents 0.6 of the shedding rate, and thus a continuum of lock-in could be expected down to one-half of the natural shedding rate (Öngoren & Rockwell 1988). As with the smooth cylinder, the case $A/D = 1.0$ reveals a second harmonic near the natural shedding rate. Perhaps more significantly, for the upper limits of lock-in, at all but the lowest amplitude, lock-in persists up to at least $f_r = 0.28$.

The wires thus give the cylinder unusual control over the total flow field, enabling this type of (peak) lock-in at very low and very high frequencies, and even at low amplitudes. The differences between the smooth and wired cylinders' lock-in during forced vibrations are most pronounced at $A/D = 0.2$, where the lock-in range is significantly expanded upwards and downwards in frequency. This expansion of the lock-in range is clear for the *present apparatus and experiments*, wherein smooth-cylinder data were obtained directly after the wire data, by simply removing the wires *in situ*. As noted above, however, Stansby (1976) and Öngoren & Rockwell (1988) have observed smooth-cylinder lock-in ranges similar to what we achieved with the wires.

Several time signals are plotted in figure 7, for the smooth cylinder and for the wired cylinder, respectively, for $A/D = 0.20$ and $f_r = 0.10$. In the case of the smooth cylinder, some force modulation is apparent because of the proximity of the forcing frequency to the shedding rate's second harmonic; the two lift forces are frequently out of alignment, and may have different magnitude. Overall, this is not a lock-in condition. When wires are added, the primary lift force component is clearly at the same frequency as the cylinder motion, although the synchronization is not complete. In addition, the lift forces at the cylinder ends are in good agreement with each other, indicating a stable vortex formation process that spans the entire cylinder. Both of the anemometer traces in figure 7, showing velocity v', illustrate the difficulty of computing dominant frequency or phase in the wake.

Several additional points are noted. For the tests at low f_r and $A/D = 0.1$, the cylinder with wires does not show a frequency increase commensurate with the

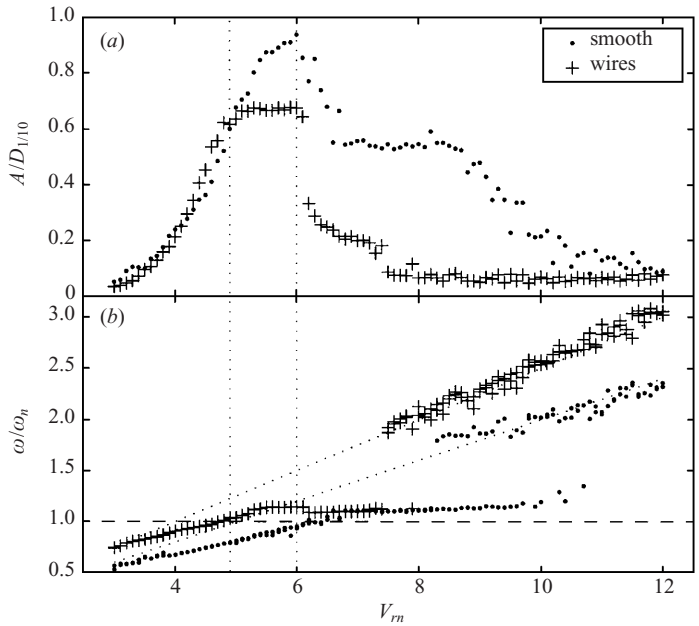

FIGURE 8. VIV response of cylinders with and without wires. The plot gives non-dimensional amplitude $A/D_{1/10}$ (*a*) and non-dimensional peak frequencies (*b*). Anemometer and lift force frequencies are shown, along with the lines $0.20V_{rn}$ and $0.25V_{rn}$. Below lock-in, the motion frequency (not shown) tracks the others; beyond the onset of lock-in, it persists near $1.13\omega_n$.

increase in Strouhal number. This observation is true for both the lift and anemometer frequencies. In a set of experiments not shown here, with $Re = 3.8 \times 10^4$, we did recover a non-dimensional frequency close to ω_S for the wires, which is the expected result for small A/D. From figure 3, it can be seen that the present tests are in a transition range, where the Strouhal number has not yet taken its terminal value near $St = 0.25$–0.27. It has not, however, remained at the the smooth cylinder value either for $Re = 3.0 \times 10^4$. This suggests that even small oscillations away from the lock-in range are sufficient to obviate the wire effects in this artificial transition regime. At higher Re, where the wire properties are stationary, one could expect some increase in non-lock-in frequency.

Figure 6 shows that the frequency range over which lock-in occurs is substantially altered by the wires. In addition, the close relation typically observed between the onset of lock-in and sharp changes in the phase and magnitude of the lift force is absent when wires are introduced. On the smooth cylinder at $A/D = 0.2$ for example, the advent of lock-in on the frequency axis (near 0.17) closely corresponds with a substantial change in phase angle. For the cylinder with wires, lock-in occurs at a frequency well below that of the smooth cylinder (0.12), and yet the sharp changes in ϕ_F and ϕ_A move to *higher* frequencies, approximately 0.19. Hence, with wires the advent of lock-in is *not* correlated with the usual changes in lift phase and magnitude, and in fact these may be unrelated phenomena. Compared to Stansby (1976) and Öngoren & Rockwell (1988), once again the effect of the wires is not as dramatic.

3.4. *Free vibrations*

VIV experiments were performed for the condition $Re = 3.0 \times 10^4$, achieving an effective damping ratio of 3.2%, as described in § 2.2.

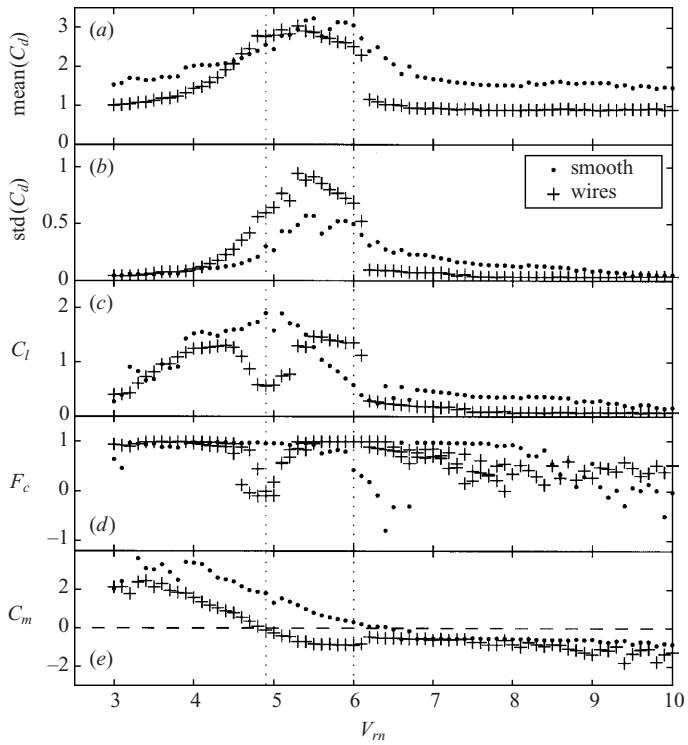

FIGURE 9. As figure 8, but for (*a*) mean drag coefficient mean(C_d), (*b*) oscillating drag coefficient std(C_d), (*c*) total lift coefficient C_l, (*d*) correlation of end lift forces F_c, and (*e*) added mass coefficient C_m.

The aggregate results are plotted in figures 8 and 9, showing results against the nominal reduced velocity, $V_{rn} = 2\pi U/\omega_n D$. The response for the smooth cylinder consists of first a gradual increase in amplitude as V_{rn} increases, with $\phi_F \approx 0°$, then a transition in ϕ_F from near 0° to near 180°, concurrent with a decline from the maximum amplitude beginning at $V_{rn} = 6.0$, then a plateau in amplitude, and finally, a gradual decrease. The wires fundamentally change the response for reduced velocities above $V_{rn} = 5.0$. Namely, the peak amplitudes reached by the smooth cylinder are never attained, but instead a plateau with $A/D_{1/10} \approx 0.69$ is observed. At $V_{rn} = 6.0$ a sharp reduction in amplitude occurs, followed closely by extremely low values, with $A/D_{1/10} < 0.1$, for $V_{rn} > 7.5$. Overall, about one half of the area under the vortex-resonance amplitude curve is eliminated by the wires.

Before we discuss the wire effects in more detail, some results for the smooth cylinder deserve explanation. The gradual phase transitions here differ with wind-tunnel and water-tunnel experimental results, in which there are two hysteretic paths, depending on whether the reduced velocity is increasing or decreasing. The difference can be explained in large part by the episodic nature of our tests, in which continuous variations in speed are not possible. In any event, the shift in ϕ_F occurs simultaneously with lock-in, defined for free vibrations as the condition $\omega \simeq \omega_n$, and also with a momentary drop in force correlation from near unity values to near zero, at $V_{rn} \approx 6.5$. The loss of force correlation indicates a potential role of three-dimensional flow; the high correlation is recovered above the phase transition.

The lift phase angles (figure 10) exhibit a similar transition from near zero to near

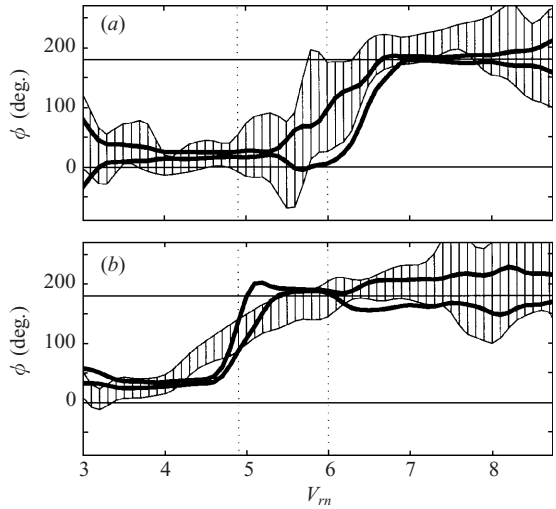

FIGURE 10. Phase angles during free vibrations. Heavy solid lines show the mean value of ϕ_F plus or minus one standard deviation. The hatched region denotes the identical spread for ϕ_A. (*a*) Smooth, (*b*) wires.

180° as the reduced velocity increases, for the cylinder with wires. The transition is shifted to lower V_{rn} with wires, however, and this event is notable in figure 8 as the point where $A/D_{1/10}$ diverges from the smooth cylinder curve, and also where ω/ω_n reaches unity. The increased frequency which allows the wired cylinder to lock in earlier is qualitatively in agreement with the slightly higher Strouhal number exhibited during stationary-cylinder tests. The slope of the frequency with V_{rn} is, however, almost identical to that of the smooth cylinder. The occurrence of $\omega/\omega_n = 1$ at low V_{rn} is due to a steady offset, which has the value $\omega/\omega_n = 0.21$ and persists for $3.0 \leqslant V_{rn} \leqslant 5.2$.

For both cylinders, the frequency ratio continues to rise from the value of 1 to the true 'locked-in' frequency ratio value of about 1.13, which is typical for tests in water and $m^* = 3.0$. By comparison, the formula given by Govardhan & Williamson (2000) predicts a value of 1.27, but that is with significantly lower damping. Figure 8 shows both anemometer and lift force frequencies, which are aligned at low V_{rn}. In the smooth-cylinder results, the anemometer leaves lock-in conditions near $V_{rn} = 8.3$, while the lift force follows only gradually at $V_{rn} \approx 10$. The wires introduce a different behaviour: *both* the wake and lift abruptly cease locked-in response at $V_{rn} = 7.4$, where a slight discontinuity in amplitude can also be seen. The motion frequency, not shown explicitly, is identical to ω_A and ω_F at low V_{rn} for both cylinders, but remains on the line $\omega/\omega_n \approx 1.13$ above lock-in for all of the V_{rn} considered.

Measurements of anemometer phase are difficult to interpret since both the motion and the anemometer signals possess multiple frequency components. Insofar as these calculations can be made, ϕ_A undergoes a change of nearly 180° at the same V_{rn} as does ϕ_F, for both cylinders. In the smooth case, the mean value of ϕ_A precedes that of ϕ_F, about $V_{rn} = 5.9$ versus 6.2. On either side of this transition, steady values of ϕ_A and ϕ_F indicate stable wakes. For the cylinder with wires, ϕ_F changes quite sharply at $V_{rn} \approx 4.9$. Anemometer phase ϕ_A changes much more gradually with wires, however, and the error statistics are quite good throughout; this suggests a poorly defined mode transition in the wake, which may encompass not only topological

changes, e.g. in the number of vortices per cycle, but also scaling changes, e.g. in the distance between cores. The notch in F_c, shown in figure 9, while moved to lower V_{rn} by the wires, is no wider than for the smooth cylinder. On the other hand, total lift coefficient C_l shows a pronounced minimum in the middle of the phase transition; for the smooth cylinder, phase changes coincide with the change of C_l from high to low values, which never really grow thereafter. Another indicator of a fundamental difference is the fluctuating drag std(C_d), which shows that ϕ changes during a decline for the smooth cylinder, but during an increase for the cylinder with wires. Overall, while the net transition of phase appears to be identical for both cylinders, the nature of the transition is modified by wires.

The lift phase change can occur at a different V_{rn} than the vortex phase change, for very low mass damping (Govardhan & Williamson 2000). For higher $m^*\zeta$, this distinction is generally not observed, and this is indeed the case for our apparatus: the two phase changes coincide, whether or not wires are used.

The various coefficients possess some additional interesting properties. There is a slightly higher maximum value of mean drag for the smooth cylinder, and a somewhat lower value for the cylinder with wires at high V_{rn}, since the amplitude of response is much smaller. Additionally, mean drag is reduced at low V_{rn} by the wires. The unsteady drag coefficient, in contrast, can be much larger for the cylinder with wires, over the range $V_{rn} = 4.0$–6.0. The cylinder with wires shows a sharp decline at $V_{rn} \approx 6$ and the oscillating drag thereafter remains lower than that of the smooth cylinder. The added mass coefficient C_m further reflects the shift in V_{rn} of the principle features as indicated in figure 8. At a given value of V_{rn}, the difference in C_m due to the wires can be as high as 2.0, for the range $V_{rn} = 4.0$–6.0. In terms of lift in phase with acceleration (not shown), the cylinder with wires reaches large positive values that are nowhere encountered by the smooth cylinder.

We show several time series in figure 11, to illustrate the salient characteristics of the responses with wires. The first two show the effects of the wires near the maximum amplitude of motion, $V_{rn} = 5.8$, and just before the phase transition for the smooth cylinder, but well after it has occurred in the cylinder with wires. In this condition, the smooth cylinder shows a very slight modulation in displacement, with a correlating modulation in the drag force. The oscillating component of drag is significant and regular, with two cycles for each cycle of transverse motion. The lift forces at the ends of the cylinder are well-correlated although of varying magnitude, and are in phase with the displacement. When wires are added, the response frequency increases, while its amplitude is reduced by about 20%. The phase transition is complete for this reduced velocity, and the frequency of motion is in fact locked to the faster structural mode. The mean value of drag is largely unaffected by the wires, although the oscillating component has grown by about 50%. The two end lift forces are nearly identical, with about the same magnitude as in the case of the smooth cylinder. In general, the motion and force signals are quite regular.

At $V_{rn} = 8.5$, both cylinders oscillate above the major phase change. The smooth cylinder here vibrates with a phase angle of 180°, just before F_c begins to decay. The value of A/D is about 0.55, and we observe that both mean and oscillating drag are much reduced from the pre-transition case. Again, two periods of drag forcing occupy one period of motion. The lift force is quite small, with the two end forces still in good agreement. The addition of wires at $V_{rn} = 8.5$ leads to vibrations of exceedingly low amplitude. The motion is irregular, but more notably, the lift and drag forces are uncorrelated and of very high frequency. The lift force amplitudes, as well as mean and fluctuating drag are also small, in fact as low as the values observed for the

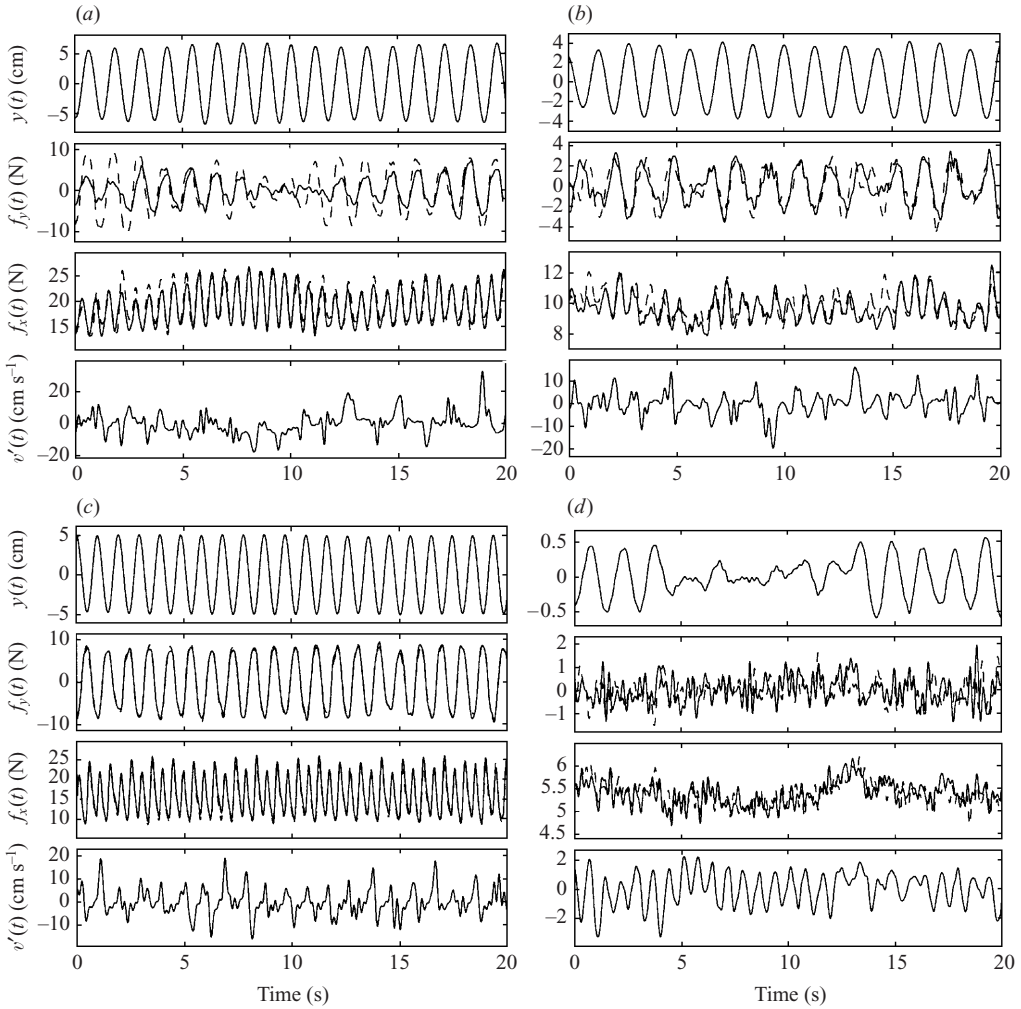

FIGURE 11. Time series for free vibrations with smooth cylinder (a, b), wired cylinder (c, d), and $V_{rn} = 5.8$ (a, c), $V_{rn} = 8.5$ (b, d).

stationary cylinder (figure 3). The high-frequency nature of the force signals suggests a significant disruption of any regular, large-scale vortex formation, and a lack of any synchronization. The anemometer and lift peak frequencies here lie on a line given by $\omega/\omega_n = 0.25V_{rn}$, signalling the end of wake lock-in for the cylinder with wires.

3.5. *Free vibrations: sensitivity to bias*

Nominal flow conditions were used in the experiments reported above, with the two wires symmetrically placed with respect to the oncoming flow. It is of importance to consider then the effect of flow perturbations causing differences in the angle of attack with respect to the wires. The effect of the wires derives from the disturbance they cause to the laminar boundary layer of the cylinder, and hence it can be expected that these effects are strongly influenced by variations in the mean direction of incident velocity. To assess this sensitivity, we performed tests with constant angular bias on the cylinder alignment, at $V_{rn} = 6.0$ and $V_{rn} = 8.0$; see figure 12. We estimate the repeatability of the rotational bias to be better than 3°.

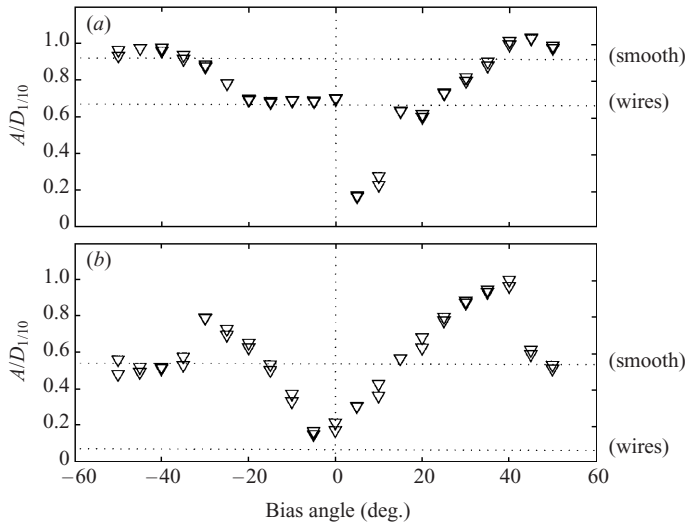

FIGURE 12. Effects of rotation angle on $A/D_{1/10}$. Horizontal lines show the levels achieved with zero bias. (*a*) $V_{rn} = 6.0$, (*b*) $V_{rn} = 8.0$.

At $V_{rn} = 6.0$ and below, the effect of the unbiased wires was found above to be a reduction in the amplitude of vibration by a moderate amount, up to 30%. When a bias angle is introduced, the dependence of peak A/D on the angle bias is non-symmetric but repeatable, with a very low value, of $A/D \simeq 0.2$, possible at around $+5°$, rotated up with respect to the oncoming flow. We initially attributed the fact that the minimum response value is obtained at non-zero bias angle to small construction misalignments of the wires used. This experiment has been repeated three times, however, with different cylinders; the same characteristic dip persists.

There are many possible causes for this sharp asymmetry. First, the proximity of the point $V_{rn} = 6.0$ to the end of the high-A/D plateau makes the response fragile to perturbations; the asymmetry may not exist for $V_{rn} = 5.5$, for example. At the same time, one would expect symmetry. The cylinder could be non-uniformly smooth, although a near mirror finish is reasonably easy to verify. The cylinder could be not perfectly round, not unlikely for stock aluminium, although again large deformities would be easy to identify. There is also the possibility of asymmetric wire placement on the cylinder, which is unlikely given the good symmetry of the bias response away from the dip, and also at $V_{rn} = 8.0$ (see below). The end-plates are circular and quite large, and we frequently checked the small gap at each end of the cylinder. Since the wires are not glued to the surface, but rather tensioned, there exists the possibility of an uneven tension due to jamming in the notches. Again, this effect would not be expected to be repeatable, and neither have we observed any vibration or loosening of wires during tests. A final asymmetry lies in the the free surface above the cylinder and the tank floor below the cylinder; the cylinder has a centred mean position, about eight diameters from either surface. Furthermore, the blockage ratio of our experiment is fairly high at 4%, and the passage of the cylinder can cause small surface waves.

Other than this significant but isolated dip, the symmetry of A/D with bias angle is as expected. Values corresponding to the zero-bias condition are maintained up to a bias of about 20°. Thereafter, the response grows to a maximum value of about 1, at a bias of 45°, after which a slight reduction seems to appear. The bias angles of

$\pm 45°$ locate one wire 25° from the mean stagnation point, and the other at 115°, well beyond the normal area of separation for a smooth stationary cylinder. However, the effects of both wires can be argued from the fact that the separation points, as well as the stagnation point, move during vibrations, and this evidently leads to the elevated amplitude. The bias at which the response is identical to the smooth cylinder case is 35°, putting the wires at 35° and 105°.

The second reduced velocity considered, $V_{rn} = 8.0$, has a zero-bias response that is significantly depressed from the smooth-cylinder value. The dependence of A/D on bias is much more regular for this case, with good symmetry to about $\pm 30°$. There exists a small bias offset of several degrees, which is within the placement error. A more significant discrepancy exists for biases greater than 30°: rotating the cylinder up toward the free surface (positive bias) extends the upward trend of the response to 40° bias, after which point the response drops to about $A/D = 0.55$, consistent with the smooth-cylinder result.

This brief sensitivity study confirms the significant effect of misalignment, as expressed through a flow bias angle. Response on the main plateau near $A/D \approx 0.70$ is not deteriorated until the bias exceeds 20°, and a dramatic localized reduction may be possible with a slight bias angle, and closely controlled flow conditions. Suppressed response on the lower plateau, at higher V_{rn}, is not as robust to bias with respect to a smooth cylinder, maintaining a useful reduction to bias angles of about $\pm 15°$.

4. Summary

For a stationary circular cylinder in crossflow, small trip wires at $\pm 70°$ from the mean stagnation point can significantly reduce drag and lift characteristics for $Re > 2 \times 10^4$, and steady conditions of reduced drag are reached in this experiment at $Re \approx 3.5 \times 10^4$. Forced-oscillation tests show that for a given amplitude of motion, the lift amplitude and phase curves as functions of reduced frequency do retain some of the main features observed in smooth cylinders, but these features are generally shifted to higher frequencies. At $A/D = 1.0$, the lift response is fundamentally changed: no excitation region exists at all. The wires further enable wake lock-in to the cylinder motion at unusually low frequencies, especially for low amplitudes. Phase changes which occur shortly above the lock-in boundary in a smooth cylinder, occur at an elevated frequency with wires, significantly beyond the lock-in boundary.

In free vibrations, the wires introduce a number of significant changes, as functions of the reduced velocity V_{rn}. An earlier mode transition, evidenced by the phasing of both lift force and wake velocity, occurs at lower V_{rn}, and corresponds to an early lock-in to the structural mode. For the lower reduced velocities, even below lock-in, the cylinder with wires has significantly reduced added mass compared to a smooth cylinder; the difference in C_m is about 2.0. Other properties are altered as well. The maximum response is moderately reduced for the cylinder with wires, and flat as a function of V_{rn}. At higher reduced velocities, above $V_{rn} \approx 6.0$, the response is largely eliminated by the wires, and only extremely low fluctuating lift and drag forces remain.

The amplitude response of the flexibly mounted cylinder with wires is sensitive to bias in the angle of the oncoming stream, but still robust enough for certain applications where the inflow conditions can be controlled to some extent. On the other hand, the application of this technique to VIV-suppression should be examined for arrangements with more wires, for example, five wires spaced at 72° or six wires at 60°.

This work is supported by the Office of Naval Research (Ocean Engineering Division), under grant number N00014-95-1-0106, monitored by Dr T. F. Swean Jr. We also thank R. Bryant and F. Gillebo for assistance with preparing and running previous sets of tests.

REFERENCES

Bearman, P. W. 1969 On vortex shedding from a circular cylinder in the critical Reynolds number regime. *J. Fluid Mech.* **37**, 577–585.

Bishop, R. E. D. & Hassan, A. Y. 1964 The lift and drag forces on a circular cylinder oscillating in a flowing fluid. *Proc. R. Soc. Lond.* A **377**, 51–75.

Brika, D. & Laneville, A. 1993 Vortex-induced vibrations of a long flexible circular cylinder. *J. Fluid Mech.* **250**, 481–508.

Fage, A. & Warsap, J. H. 1929 The effects of turbulence and surface roughness on the drag of a circular cylinder. *Aero. Res. Comm. R. & M.* No. 1283.

Feng, C. C. 1968 The measurement of vortex-induced effects in flow past stationary and oscillating circular and D-section cylinders. MASc Thesis, University of British Columbia.

Fung, Y. C. 1960 Fluctuating lift and drag acting on a cylinder in a flow at supercritical Reynolds numbers. *J. Aero. Sci.* **27**, 801–814.

Gopalkrishnan, R. 1992 Vortex-induced forces on oscillating bluff cylinders. ScD Dissertation, Massachusetts Institute of Technology/Woods Hole Oceanographic Institution Joint Program in Oceanographic Engineering.

Govardhan, R. & Williamson, C. H. K. 2000 Modes of vortex formation and frequency response of a freely vibrating cylinder. *J. Fluid Mech.* **420**, 85–130.

Hover, F. S., Techet, A. H. & Triantafyllou, M. S. 1998 Forces on oscillating uniform and tapered cylinders in crossflow. *J. Fluid Mech.* **363**, 97–114.

Hover, F. S. & Triantafyllou, M. S. 1999 Combined simulation with real-time force feedback: A new tool for experimental fluid mechanics. In *System Theory: Modeling, Analysis, and Control* (ed. T. E. Djaferis & I. C. Schick). Kluwer.

Igarashi, T. 1986 Effect of tripping wires on the flow around a circular cylinder normal to an airstream. *Bull. Japan. Soc. Mech. Engng* **29**, 2917–2924.

James, D. F. & Truong, Q. S. 1972 Wind load on cylinder with spanwise protrusion. *Proc. ASCE, J. Engng Mech. Div.* **98**, 1573–1589.

Jones, G. W. Jr, Cincotta, J. J. & Walker, R. W. 1968 Aerodynamic forces on a stationary and oscillating circular cylinder at high Reynolds numbers. *NASA Langley Tech. Rep.* 124-08-04-22-23.

Karniadakis, G. E. & Triantafyllou, M. S. 1989 Frequency selection and asymptotic states in laminar wakes. *J. Fluid Mech.* **199**, 441–469.

Khalak, A. & Williamson, C. H. K. 1996 Fluid forces and dynamics of a hydroelastic structure with very low mass and damping. *J. Fluids Struct.* **11**, 973–982.

Öngoren, A. & Rockwell, D. 1988 Flow structure from an oscillating cylinder. Part 1. Mechanisms of phase shift and recovery in the near wake. *J. Fluid Mech.* **191**, 197–223.

Pearcey, H. H., Cash, R. F. & Salter, I. J. 1982 Flow past circular cylinders: Simulation of full-scale flows at model scale. *NMI Rep.* 131.

Price, P. 1956 Suppression of the fluid-induced vibration of circular cylinders. *Proc. ASCE, J. Engng Mech. Div.* **82**, Paper 1030.

Ribeiro, J. L. D. 1991 Effects of surface roughness on the two-dimensional flow past circular cylinders, I: Mean forces and pressures. *J. Wind Engng Indust. Aerodyn.* **37**, 299–309.

Romberg, O. & Popp, K. 1998 The influence of trip-wires on the fluid-damping-controlled instability of a flexible tube in a bundle. *J. Fluid Struct.* **12**, 17–32.

Roshko, A. 1961 Experiments on the flow past a circular cylinder at very high Reynolds number. *J. Fluid Mech.* **10**, 345–356.

Sarpkaya, T. 1977 Transverse oscillations of a circular cylinder in uniform flow. *Tech. Rep.* NPS-69SL77071-R. Naval Postgraduate School, Monterey, CA.

Schewe, G. 1983 On the force fluctuations acting on a circular cylinder in crossflow from subcritical up to transcritical Reynolds numbers. *J. Fluid Mech.* **133**, 265–285.

Schlichting, H. 1979 *Boundary-Layer Theory*. McGraw-Hill.

Shih, W. C. L., Wang, C., Coles, D. & Roshko, A. 1993 Experiments on flow past rough circular cylinders at large Reynolds numbers. *J. Wind Engng Indust. Aerodyn.* **49**, 351–368.

Stansby, P. K. 1976 The locking-on of vortex shedding due to the cross-stream vibration of circular cylinders in uniform and shear flows. *J. Fluid Mech.* **74**, 641–665.

Techet, A. H., Hover, F. S. & Triantafyllou, M. S. 1998 Vortical patterns behind tapered cylinders oscillating transversely to a uniform flow. *J. Fluid Mech.* **363**, 79–96.

Williamson, C. H. K. & Roshko, A. 1988. Vortex formation in the wake of an oscillating cylinder. *J. Fluids Struct.* **2**, 355–381.

Zdravkovich, M. M. 1981 Review and classification of various aerodynamic and hydrodynamic means for suppressing vortex shedding. *J. Wind Engng Indust. Aerodyn.* **7**, 145–189.